Journal of Energy Storage 38 (2021) 102538

Contents lists available at ScienceDirect

Journal of Energy Storage

journal homepage: www.elsevier.com/locate/est

Natural convection from a bottom heated of an asymmetrical U-shaped enclosure with nano-encapsulated phase change material

H. Saleh [a,*], Z. Siri [b], M. Ghalambaz [c,d]

[a] Mathematics Education Department, Universitas Islam Negeri Sultan Syarif Kasim Riau, 28293, Pekanbaru, Indonesia
[b] Institute of Mathematical Sciences, University of Malaya, 50603, Kuala Lumpur, Malaysia
[c] Faculty of Applied Sciences, Ton Duc Thang University, Ho Chi Minh City, Viet Nam
[d] Metamaterials for Mechanical, Biomechanical and Multiphysical Applications Research Group, Ton Duc Thang University, Ho Chi Minh City, Viet Nam

ARTICLE INFO

Keywords:
Free convection
Hybrid nanofluids
NEPCM particles
Phase change heat transfer
U-shaped

ABSTRACT

In the current study, free convection of a hybrid nanofluid in asymmetrical U-shaped enclosure is studied numerically. The bottom plate is heated and the top U-shaped walls is cooled, while the other walls are insulated. The cold basin moves along the horizontal centerline that measure the asymmetrically shape. The hybrid nanofluid is formed of a phase-change material (PCM) suspended in the water. The PCM utilize polyurethane as the protective case and nonadecane inside. The core absorb or release thermal energy in the shape of latent heat. The nanoparticle concentration, asymmetrical parameter, aspect ratio, fusion temperature and Rayleigh number have been investigated in detail. The results shows that the global heat transfer performance can be enhanced more than 9% by adding 1% nano-capsules volume fraction. Symmetry U-shaped does not give the maximum heat transfer performance and changing the basin location has small effect the heat transfer enhancement at moderate aspect ratio and fusion temperature.

1. Introduction

Nanoscience and nanotechnology deal with ultra tiny things which enable us to visual and design the bonds among atoms inside materials. Choi [1] introduced the human-made nanoparticles inside the base fluid to increase heat transfer of the thermal system. Latest technological method is Nano-Encapsulated Phase Change Materials or called as NEPCMs. This innovative technique separate outer shell material and inner core material. The inner material is PCM with a specific fusion temperature. It enables to absorbs or releases a large energy from the latent heat [2]. Fang et al. [3] introduced the NEPCMs composed in situ polymerization techniques. They utilized the n-tetradecane as the core and carbamide and formaldehyde for the protective case. Sodium dodecyl sulfate was utilized as the stabilizer and resorcin was utilized as the subtract modifier. Jamekhorshid et al. [4] summarized the techniques used for microencapsulated phase change materials (MEPCMs). Shchukina et al. [5] reviewed the several techniques used for the encapsulation PCMs for new product of energy storage systems. Nazir et al. [6] discussed the ideas in improving the heat storage that utilize the PCMs through encapsulation.

Natural convection in enclosure occurs when the heat generated by the heating wall or object inside that bring to the fluid movement. This convection type is designed to exchange the heat and handle the thermal management. Abundant works were conducted in studying the fluid movement and heat transfer in arbitrary enclosures with several thermal boundary conditions type and operating fluids. Morsi and Das [7], discussed effect of waviness in the complex enclosures. Different operating fluids, nanofluids, was found by Khanafer et al. [8] to considerably enhance the heat transfer rate. Later, Jou and Tzeng [9] utilized the different nanofluids type and they obtained the heat transfer enhancement.

Non-rectangular enclosure in the form of T-shape was studied by El-Alami et al. [10]. Amraqui et al. [11] found that increasing of heating intensity and the considering the radiation exchange produce significantly increase in the heat transfer. Kasaeipoor et al. [12] studied magnetohydrodynamic combined convection of a nanofluid in a vented T-shaped enclosure. Armaghani et al. [13] found that Nusselt number globally increases with the larger baffle size and larger Hartmann number reduced the entropy production. Non-rectangular enclosure in the form of C-shape was studied by Chamkha et al. [14]. They studied the entropy generation in a C-shaped enclosure having nanofluid under effect of uniform magnetic field. Mliki et al. [15] reported the heat transfer increases if the Brownian motion effect takes into consideration. Mohebbi et al. [16] found the highest Nusselt number was obtained if the heat source was put in the upper horizontal of the

* Corresponding author.
E-mail address: Dr.habibissaleh@gmail.com (H. Saleh).

https://doi.org/10.1016/j.est.2021.102538
Received 31 December 2020; Received in revised form 17 March 2021; Accepted 4 April 2021
Available online 13 April 2021

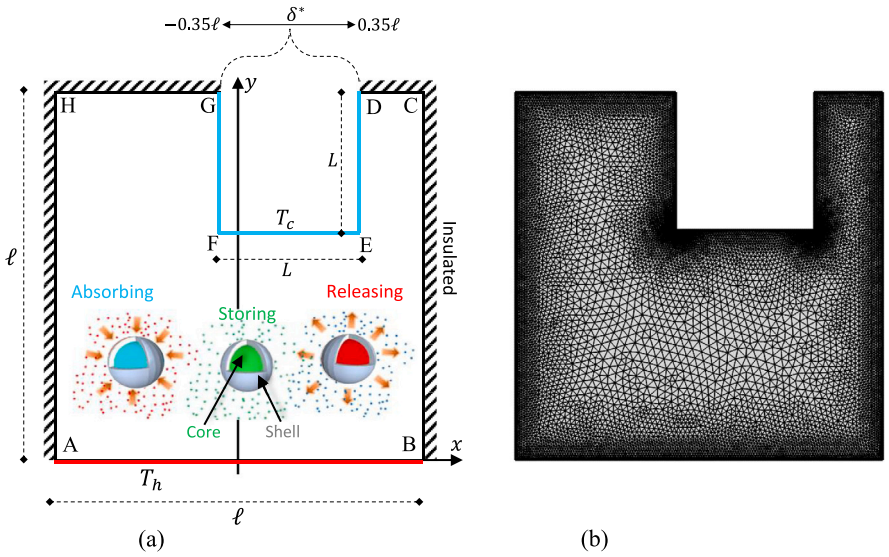

Fig. 1. (a) Schematic representation of an asymmetric U-shaped enclosure filled with a hybrid nanofluid, (b) Grid distribution.

C-shaped enclosure. Aghakhani et al. [17] considered non-Newtonian fluid in a C-shaped enclosure and concluded the Nusselt number decreases with increasing cavity aspect ratio. Abedini et al. [18] found that the heat transfer enhancement was more noticeable by increasing the aspect ratio. Non-rectangular enclosure in the form of H-shaped was studied by Rahimi et al. [19]. They illustrated the local maps of fluid friction and heat transfer in H-shaped irreversibility. Purusothaman and Malekshah [20] studied natural convection in a tilted V-shaped electronic device filled with Cu–water nanofluid.

Non-rectangular enclosure in the form of L-shaped was studied by Kalteh and Hasani [21]. They concluded that improvement of the thermal performance is greater for lower aspect ratios. Elshehabey et al. [22] found the existing of the magnetic field produces a considerably reduction in the fluid flow and heat transfer performed. Mohebbi and Rashidi [23] investigated L-shaped enclosure having a hot obstacle and found reducing thermal performance by increasing the aspect ratio and the reducing is more pronounced in the low Rayleigh number. Rahimi et al. [24] considered the hollow L-shaped cavity is considered and filled with hybrid nanofluid. The viscosity together with the conductivity were calculated experimentally. Gawas and Patil [25] observed free convection in the L-shaped enclosure heated from below at low Rayleigh numbers. Different configuration was investigated by Cho et al. [26] considering nanoliquid in a U-shaped enclosure. Ma et al. [27] studied nanofluid in a U-shaped enclosure having a heating body. Heat transfer enhancement is found by Snoussi et al. [28] to enhance by adding nanoparticles volume fractions, heating intensity and cooled wall length extensions. Ma et al. [29] considered the bottom wall heating and adopt the Koo–Kleinstreuer–Li formulation to predict the thermophysical properties of the nanoliquid.

Single or hybrid nanofluids on melting process in vertically heating of the square enclosure filled with nano-enhanced PCM was initially started by Sebti et al. [30]. Then, Ho and Gao [31] experimentally studied this configuration. Tasnim et al. [32] investigated the convection influence on the melting process of the new type of PCM inside the porous enclosure. The exergy efficiency was reached up 22% when the heat storage enclosure filled with the PCM [33]. Dhaidan [34] considered several types of the enclosures such as rectangular and found that the nanostructures assist the heat transfer. Ghalambaz et al. [35] demonstrated that the hybrid nanoparticles enhance fusion performance of nano-enhanced PCM in a square enclosure. Ghalambaz et al. [36] studied the PCM in an enclosure heated vertically from the bottom. They found modification of the conductivity and viscosity parameters bring alteration in the liquid fraction. Motahar et al. [37] showed that the conduction mode occurs at the beginning melting and at later replaced by natural convection. Al-Jethelah et al. [38] compared melting processes between pure PCM and mixture PCM. Selimefendigil et al. [39] studied conjugate convection characteristic of nanofluid in a square enclosure where a PCM installed on the side wall subject to an inclined magnetic field. Bondareva et al. [40] reported that nano PCM melts earlier for the orientation angle greater than 90 degree at high heating intensity. Iachachene et al. [41] concluded that maximum melting rate was obtained by adjusting the trapezoidal enclosure orientation. Selimefendigil and Oztop [42] studied a square cavity filled with PCM and a rotating cylinder put in the center. Ghalambaz et al. [43] and Hajjar et al. [44] studied the heat transfer improvement of NEPCMs in a differentially heated enclosure. Thermal energy storage utilizing PCM nano encapsulation technology takes advantages of harvesting energy compared to nano-enhanced PCM technology. Zadeh et al. [45] found that the high entropy generation in a square enclosure at high the nano-capsules concentration. Thermal performance was reported by Mehryan et al. [46] to increase by taking large difference of the core fusion temperature and the walls temperature. Ghalambaz and Zhang [47] demonstrated that the PCM heatsink increases the thermal performance especially at small Biot number.

Most of the previous studies regarding the investigation of the NEPCM hybrid nanofluids are subject to rectangular enclosure, but in practical situations still be subject to free convection strategy on removing the heat and managing the thermal systems. The present work is the first investigation on the application of NEPCM with main purpose to enhance the heat transfer in an U-shaped enclosure. This work aims to answer the questions: how does the fluid react to the pulse heat load by melting or solidification and what is the optimal configuration for the best heat transfer. The main parameters in this simulation are Rayleigh number, solid volume fraction, fusion temperature, aspect ratio and asymmetric parameter. Symmetrical U-shaped is simple enclosure styles and easily fabricated. Symmetry issue is an important property of the commercial heat exchangers for thermal energy storage. It may be displayed in more pleasant or artful appearance of the heat exchanger shape. However, if the enclosure needs to accommodate a certain component that protrudes from opposite sides then the symmetrical style is not going to work.

2. Mathematical formulation

A schematic model of an asymmetric U-shaped cavity filled with a hybrid nanofluid in Fig. 1(a). The enclosure with size ℓ. Bottom wall

Table 1
The thermophysical properties of the applied materials [48].

Materials	ρ (kg/m^3)	μ (N s/m^2)	k (W m^{-1} K^{-1})	C_p (J/kg K)	β (1/K)
Water	997.1	0.00089	0.613	4.1790	0.00021
Polyurethane	786	–	–	1.3177	0.0001728
Nonadecane	721	–	–	2.0370	–

has temperature, T_h. The top U-shaped walls have constant temperature, T_c and the other surfaces are adiabatic. Symbol δ^* in the figure is a distance from vertical centerline of the enclosure to the center of U-shaped basin. The δ^* moves along the horizontal centerline from -0.35ℓ to 0.35ℓ. The bottom surface and the top U-shaped surfaces subject to the gravitational acceleration at different temperature level bring to natural convection problem.

The NEPCMs are made of a phase-change materials. This advanced material contains an outer shell and a core inside. The outer shell is polyurethane and the core is nona-decane. The thermophysical properties of the applied materials is tabulated in Table 1. The inner subjects to a phase change to fluid in the fusion temperature interval with $T_h < T_f < T_c$. The phase change temperature and the latent heat of the inner core are 305 (K) and 211 (kJ/kg), respectively. Specifically, the PCM core of the hybrid nanoparticles can absorb/release a notable amount of energy in the form of latent heat. Moreover, the latent heat of the nanoparticle cores can contribute in energy transport inside the host fluid. The suspension of NEPCMs and a host fluid is assumed to be uniform and stable. Based on these considerations, the continuity, momentum and energy equations can be stated as follows [43,44]:

$$\frac{\partial u}{\partial x} + \frac{\partial v}{\partial y} = 0 \tag{1}$$

$$\rho_b \left(u\frac{\partial u}{\partial x} + v\frac{\partial u}{\partial y} \right) = -\frac{\partial p}{\partial x} + \mu_b \left(\frac{\partial^2 u}{\partial x^2} + \frac{\partial^2 u}{\partial y^2} \right) \tag{2}$$

$$\rho_b \left(u\frac{\partial v}{\partial x} + v\frac{\partial v}{\partial y} \right) = -\frac{\partial p}{\partial y} + \mu_b \left(\frac{\partial^2 v}{\partial x^2} + \frac{\partial^2 v}{\partial y^2} \right) + g\rho_b\beta_b(T - T_c) \tag{3}$$

$$(\rho Cp)_b \left(u\frac{\partial T}{\partial x} + v\frac{\partial T}{\partial y} \right) = k_b \left(\frac{\partial^2 T}{\partial x^2} + \frac{\partial^2 T}{\partial y^2} \right) \tag{4}$$

Here (u,v) are velocities vector, T is temperature and p is pressure where subscript of b refers the bulk properties of the hybrid nanofluid, g is the acceleration due to gravity, μ_b, ρ_b, k_b and β_b are viscosity, the density, conductivity, thermal expansion coefficient of the base liquid at room temperature, respectively.

The density of the mixture is written as a weighted relation of the water and NEPCM dispersed particles:

$$\rho_b = (1 - \phi)\,\rho_f + \phi\rho_p \tag{5}$$

The p and f symbols are NEPCM particles and the water, respectively.

The density of NEPCM material is defined as follows:

$$\rho_p = \frac{(1 + \imath)\,\rho_{co}\rho_{sh}}{\rho_{sh} + \imath\rho_{co}} \tag{6}$$

where ρ_{sh} is density of the shell while ρ_{co} is density of the core. $\imath$ is the core–shell mass ratio and is about $\imath \sim 0.447$ [48]. Furthermore, the density of the core is the mean of the fluid and solid phases of the phase change material. The specific heat capacitance of the suspension can be evaluated as:

$$C_{p,b} = \frac{(1 - \phi)(\rho C_p)_f + \phi(\rho C_p)_p}{\rho_p} \tag{7}$$

The specific heat capacitance subject to no phase change, $C_{p,p}$ is evaluated by the following function:

$$C_{p,p} = \frac{(C_{p,co} + \imath C_{p,sh})\rho_{co}\rho_{sh}}{(\rho_{sh} + \imath\rho_{co})\rho_p} \tag{8}$$

It notes that the heat capacity of the core is the mean of the heat capacities of the fluid and solid phases. This due to the nanoparticles core subject to solid and fluid phase then the latent heat was engaged in the heat capacity of the NEPCM. This heat can be formulated by performing rectangular, triangular or trigonometric functions as follows [49]:

$$C_{p,p} = C_{p,co} + \frac{h_{sf}}{T_{Mr}} \tag{9}$$

$$C_{p,p} = C_{p,co} + \left\{ \frac{\pi}{2} \cdot \left(\frac{h_{sf}}{T_{Mr}} - C_{p,co} \right) \cdot \sin\left(\pi \frac{T - T_{fu} + \frac{T_{Mr}}{2}}{T_{Mr}} \right) \right\} \tag{10}$$

$$C_{p,p} = C_{p,co} + 2\left(\frac{h_{fs}}{T_{Mr}^2} - \frac{C_{p,co}}{T_{Mr}} \right) \left(T - T_{fu} + \frac{T_{Mr}}{2} \right) \tag{11}$$

Symbol T_{Mr} denotes the temperature range. In fact, this range prevents the discontinuity in energy equilibrium. The total heat capacity of the NEPCM core including the sensible together with latent heats are evaluated based on T_{Mr}:

$$C_{p,p} = C_{p,co} + \left\{ \frac{\pi}{2} \cdot \left(\frac{h_{sf}}{T_{Mr}} - C_{p,co} \right) \cdot \sin\left(\pi \frac{T - T_{fu} + \frac{T_{Mr}}{2}}{T_{Mr}} \right) \right\} \gamma \tag{12}$$

where

$$\gamma = \begin{cases} 0 & T < T_{fu} - \frac{T_{Mr}}{2} \\ 1 & T_{fu} - \frac{T_{Mr}}{2} < T < T_{fu} + \frac{T_{Mr}}{2} \\ 0 & T > T_{fu} + \frac{T_{Mr}}{2} \end{cases} \tag{13}$$

The thermal expansion coefficient of the mixture is written as

$$\beta_b = (1 - \phi)\,\beta_f + \phi\beta_p \tag{14}$$

The functions showed below are performed to evaluate the thermal conductivity of mixture having of nano-encapsulated PCM:

$$\frac{k_b}{k_f} = 1 + Nc\phi \tag{15}$$

The dynamic conductivity of suspension:

$$\frac{\mu_b}{\mu_f} = 1 + Nv\phi \tag{16}$$

Nc and Nv of the above equations refers to the coefficients of conductivity and viscosity, respectively. These non-dimensional parameters, Nc and Nv, are generally functions of the size, shape and constructing materials of the nanoparticles, the type of the base fluid, the working temperature and other affective parameters. The parameters Nc and Nv can be extracted using linear curve fitting on the available experimental data. In this work, we have used experimental data of Barlak et al. [48]. It notes that these functions are valid only for diluted nanofluids when $\phi < 0.05$.

We introduce the following non-dimensional quantity:

$$X = \frac{x}{\ell},\ Y = \frac{y}{\ell},\ \delta = \frac{\delta^*}{\ell},\ AR = \frac{L}{\ell},\ U = \frac{u\ell}{\alpha_f}$$

$$V = \frac{v\ell}{\alpha_f},\ P = \frac{p\ell^2}{\rho_f\alpha_f^2},\ \Theta = \frac{T - T_c}{T_h - T_c} \tag{17}$$

The non dimensional form of the governing equations become:

$$\frac{\partial U}{\partial X} + \frac{\partial V}{\partial Y} = 0 \tag{18}$$

$$\left(\frac{\rho_b}{\rho_f} \right) \left(U\frac{\partial U}{\partial X} + V\frac{\partial U}{\partial Y} \right) = -\frac{\partial P}{\partial X} + Pr \left(\frac{\mu_b}{\mu_f} \right) \left(\frac{\partial^2 U}{\partial X^2} + \frac{\partial^2 U}{\partial Y^2} \right) \tag{19}$$

$$\left(\frac{\rho_b}{\rho_f} \right) \left(U\frac{\partial V}{\partial X} + V\frac{\partial V}{\partial Y} \right) = -\frac{\partial P}{\partial Y} + Pr \left(\frac{\mu_b}{\mu_f} \right) \left(\frac{\partial^2 V}{\partial X^2} + \frac{\partial^2 V}{\partial Y^2} \right) + RaPr\frac{(\rho\beta)_b}{(\rho\beta)_f}\Theta \tag{20}$$

$$Cr \left(U\frac{\partial \Theta}{\partial X} + V\frac{\partial \Theta}{\partial Y} \right) = \frac{k_b}{k_f} \left(\frac{\partial^2 \Theta}{\partial X^2} + \frac{\partial^2 \Theta}{\partial Y^2} \right) \tag{21}$$

The non dimensional form of boundary conditions become:

$$U = V = 0,\ \ \frac{\partial \Theta}{\partial n} = 0 \text{ on segments BC, CD, GH and HA,} \tag{22}$$

$$U = V = 0,\ \Theta = 1 \text{ on segment AB,} \tag{23}$$

$$U = V = 0,\ \Theta = 0 \text{ on segments DE, EF and FG,} \tag{24}$$

The δ is a non dimensional distance from vertical centerline, Cr is the ratio of heat capacity of the mixture to the sensible heat capacity of the water and AR is the aspect ratio. The Rayleigh number, Ra and Prandtl number, Pr are non dimensional quantities defined as:

$$Ra = \frac{g\rho_f \beta_f \Delta T \ell^3}{\alpha_f \mu_f},\ Pr = \frac{\mu_f}{\rho_f \alpha_f} \tag{25}$$

Also,

$$\left(\frac{\rho_b}{\rho_f}\right) = (1-\phi) + \phi\left(\frac{\rho_p}{\rho_f}\right),\ \left(\frac{\beta_b}{\beta_f}\right) = (1-\phi) + \phi\left(\frac{\beta_p}{\beta_f}\right) \tag{26}$$

It is considered that the thermal expansion of the NEPCMs are equal to the water and therefore, $\beta_b/\beta_f \sim 1$. The Cr is defined as:

$$Cr = \frac{(\rho C_p)_b}{(\rho C_p)_f} = (1-\phi) + \phi\lambda + \frac{\phi}{\delta Ste} f \tag{27}$$

the sensible heat capacity ratio λ, the melting interval ε and Stephan number Ste can be stated as follows:

$$\lambda = \frac{\left(C_{p,co} + \imath C_{p,sh}\right)\rho_{co}\rho_{sh}}{(\rho C_p)_f\left(\rho_{sh} + \imath\rho_{co}\right)} \tag{28}$$

$$\varepsilon = \frac{T_{Mr}}{\Delta T} \tag{29}$$

$$Ste = \frac{(\rho C_p)_f \Delta T\left(\rho_{sh} + \imath\rho_{co}\right)}{\alpha_f\left(h_{sf}\rho_{co}\rho_{sh}\right)} \tag{30}$$

In addition, f, the fusion relation, is stated as:

$$f = \frac{\pi}{2}\sin\left(\frac{\pi}{\varepsilon}\left(\Theta - \Theta_{fu} + \frac{\varepsilon}{2}\right)\right)\sigma \tag{31}$$

where

$$\sigma = \begin{cases} 0 & \Theta < \Theta_{fu} - \frac{\varepsilon}{2} \\ 1 & \Theta_{fu} - \frac{\varepsilon}{2} < \Theta < \Theta_{fu} + \frac{\varepsilon}{2} \\ 0 & \Theta > \Theta_{fu} + \frac{\varepsilon}{2} \end{cases} \tag{32}$$

Here, Θ_{fu}, the non-dimensional fusion temperature, is:

$$\Theta_{fu} = \frac{T_{fu} - T_c}{\varepsilon T} \tag{33}$$

The local Nusselt number calculated at the hot wall is

$$Nu = -(1 + Nc\phi)\frac{\partial\Theta}{\partial Y} \tag{34}$$

The averaged Nusselt number at the hot wall is calculated as

$$\overline{Nu} = \int_{-0.5}^{0.5} Nu\,dY \tag{35}$$

3. Solution method

The non-dimensional governing equations was solved by the Galerkin weighted residual FEM, Comsol solver. By default Comsol is set up to do physics and most engineers use dimensional form in their computation. Comsol also support several PDE Interfaces of adding elliptic, hyperbolic, or parabolic PDE equations with constant or non-constant coefficients. This Mathematics interfaces were applied here and discussion about how to apply the interface on solving the non dimensional form was given by Li et al. [50].

Computational domain was divided into sub-domains where the approximation of each of the velocity, pressure and temperature variables were given by Zienkiewicz et al. [51]. Computational domain is set by triangular shapes. For each of the velocity, temperature and pressure in the computational domain, different orders are applied. For the non dimensional form of the continuity, momentum and heat transfer equations, calculating of residuals is done by changing the approximations into the governing equations. A damped Newton method is applied to approximate the nonlinear terms in the governing equations.

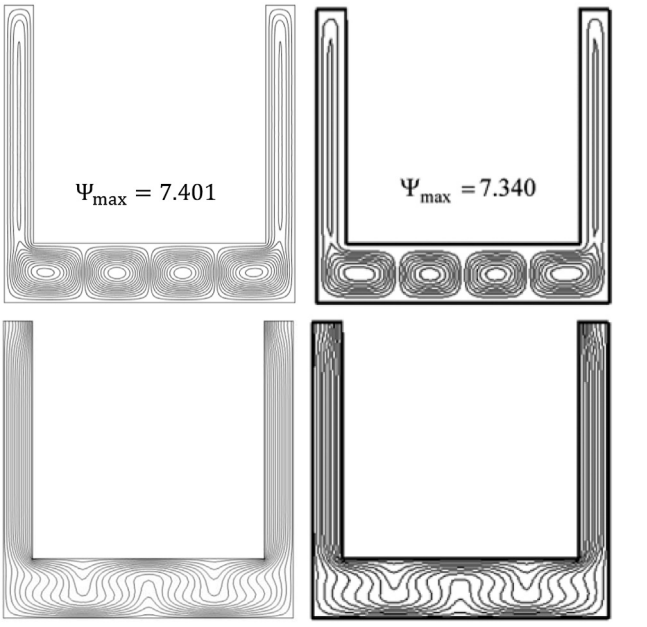

Fig. 2. Comparison of calculated streamlines and isotherms of the current work (bottom) with that of literature (top) at $Ra = 10^6$, $AR = 0.8$, $\delta = 0.5$, $\phi = 0.05$, $\theta_f = 0.0$ and the nanofluid is CuO–water.

Table 2
Grid sensitivity checks for the mean Nusselt number and the maximum value of stream function at $Ra = 5\times10^5$, $\delta = -0.1$, $\phi = 0.05$, $Ste = 0.2$, $\theta_f = 0.3$ and $AR = 0.35$.

Predefined mesh size	Domain elements	Boundary elements	$\overline{Nu}$	$\lvert\Psi\rvert_{max}$	CPU time (s)
Normal	2110	156	11.175	39.934	19
Fine	3312	194	11.023	39.842	18
Finer	8481	395	11.082	39.650	37
Extra fine	21 594	756	11.110	39.653	74
Extremely fine	29 096	756	11.090	39.637	100

Table 3
Comparison of average Nusselt number with Armaghani et al. [13] which is a natural convection of nanofluid inside of T-shaped enclosure at $Ra = 10^5$, $\phi = 0.1$.

References	$AR = 0.3$	$AR = 0.5$	$AR = 0.7$	$AR = 0.9$
Mansour et al. [53]	5.898	5.660	5.430	5.345
Armaghani et al. [13]	5.993	5.773	5.546	5.441
Present study	5.996	5.781	5.553	5.449

Different mesh sizes are compared to adopt a mesh with good accuracy and low computational cost. Meshing of the domain is conducted into a regular mesh as shown in Fig. 1(b). The mesh was stretched with the default stretching ratio near the walls to adequately capture the thermal layer, and the mesh is progressively coarsened towards the middle of the enclosure. To achieve mesh independence in COMSOL several tests were conducted on the predefined mesh sizes: normal, fine, finer, extra fine and extremely fine. For this, the average Nusselt number and the stream function values at $Ra = 5\times10^5$, $\delta = -0.1$, $\phi = 0.05$, $\theta_f = 0.3$, $Ste = 0.2$ and $AR = 0.35$ was considered. The results depicted in Table 2 suggest that an extremely fine mesh was selected. As a validation, our result for the streamline and isotherms agree well with those found by Ghasemi [52] at $Ra = 10^6$, $AR = 0.8$, $\delta = 0.5$, $\phi = 0.05$, $\theta_f = 0.0$ and the nanofluid is CuO–water as displayed in Fig. 2.

Additional validation in Table 3 is performed by a comparison with the published work of [53] and [13] which is a natural convection of

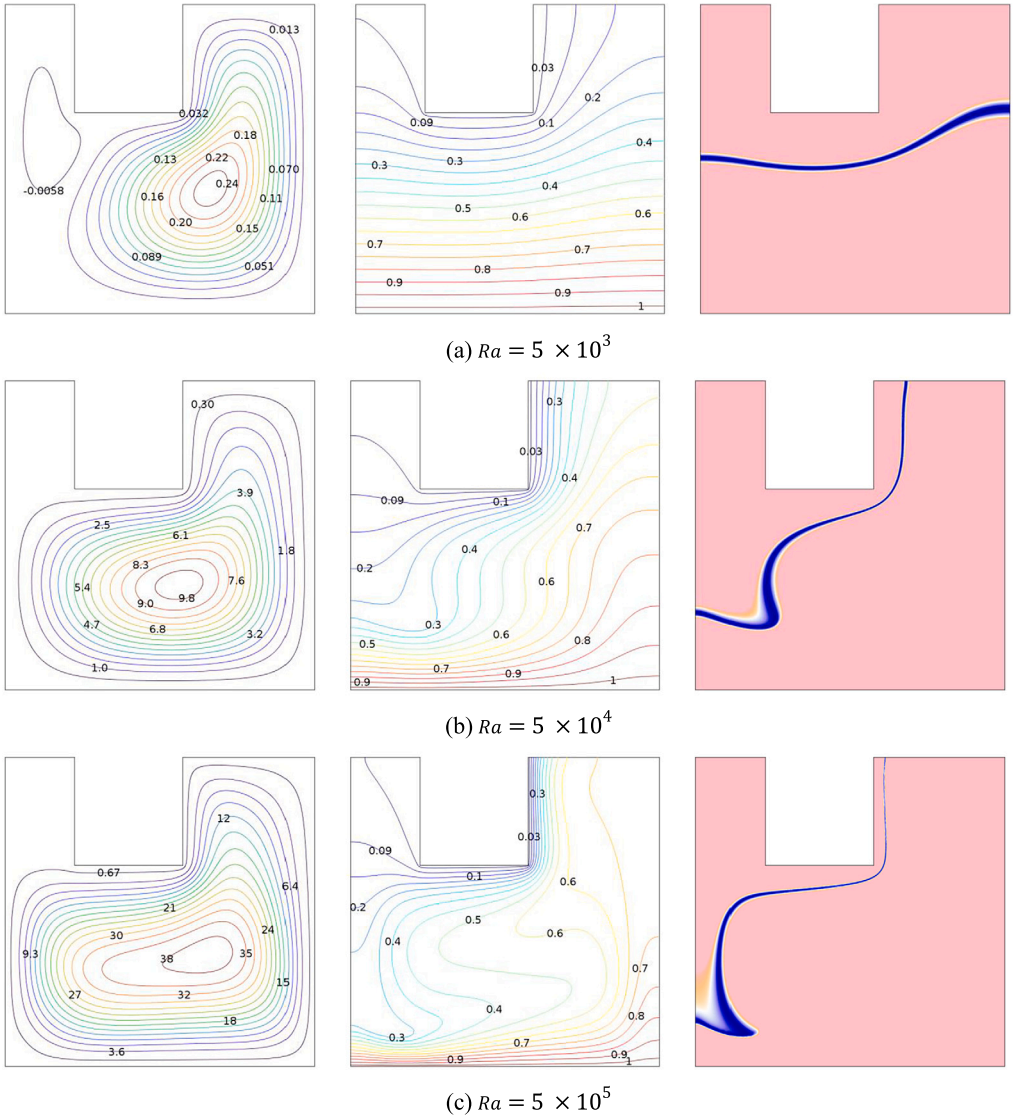

Fig. 3. Influence of the Rayleigh number on streamlines (left), isotherms (middle) and heat capacity ratio distribution (right) at $\delta = 0.4$, $\phi = 0.05$, $\theta_f = 0.3$, $Ste = 0.2$ and $AR = 0.35$.

Table 4
Comparison of average Nusselt number with Ghalambaz et al. [43] which is a natural convection of NEPCMs in a differentially heated square enclosure at $Ra = 10^5$, $\phi = 0.05$, $\lambda = 0.4$, $Nc = Nv = 3.0$.

References	$\theta_f = 0.1$ $Ste = 0.313$	$\theta_f = 0.2$ $Ste = 0.313$	$\theta_f = 0.3$ $Ste = 0.313$	$\theta_f = 0.3$ $Ste = 0.2$
Ghalambaz et al. [43]	4.9550	5.1022	5.1932	5.3541
Present study	4.9551	5.1022	5.1932	5.3542

nanofluid inside of T-shaped enclosure at $Ra = 10^5$, $\phi = 0.1$. Comparison of present result for average Nusselt number was conducted for different aspect ratio. Another comparison with the published work of Ghalambaz et al. [43] which is a natural convection of NEPCMs in a differentially heated square enclosure at $Ra = 10^5$, $\phi = 0.05$, $\lambda = 0.4$, $Nc = Nv = 3.0$ is conducted in Table 4. Comparison of present result for average Nusselt number was conducted for different fusion temperature and Stefan number. In each case, Nusselt number are equivalent with reported in the literatures. These comprehensive validations confirm the reliability of the current calculation.

4. Results and discussion

This section intends to explain the outcome of the numerical simulation for the present model, which has been given in (18)–(33). The physical interactions between the fluid and the NEPCM were conveyed through the logical manipulation of the governing parameters' values such as S (portion of the heated segment), Ra (the Rayleigh number), θ_f (fusion temperatures), ϕ (nanoparticles concentration), and Ste (Stefan number) from the aspect of streamlines, isotherms, heat capacity ratio, instantaneous Nusselt number, Nu and the mean Nusselt number, $\overline{Nu}$. Due to the core weight of the NEPCM is less than water, and shell weight is more than the base fluid, the density ratio is taken as 0.742. The value of the material, a dilute suspension of NEPCMs with $Nc = 23.8$, $Nv = 12.5$ [48]. The NEPCM were made using an interfacial polymerization technique and the melting temperature range was fixed at 0.05 with the sensible capacity ratio 0.32. The thermal expansion coefficient of the particles are small enough compare to water, in addition the volume fraction of the particles are low.

Fig. 3 shows the development of the streamlines, isotherms and heat capacity ratio distribution by increasing the Rayleigh number at $\delta = 0.4$, $\phi = 0.05$, $\theta_f = 0.3$, $Ste = 0.2$ and $AR = 0.35$. When the Rayleigh

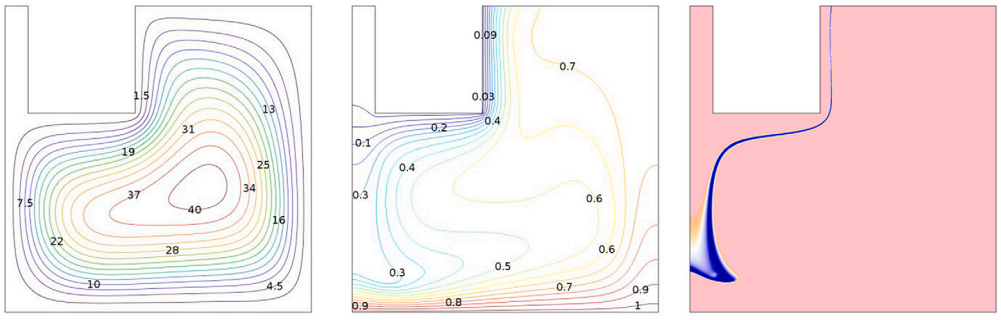

(a) δ = -0.25

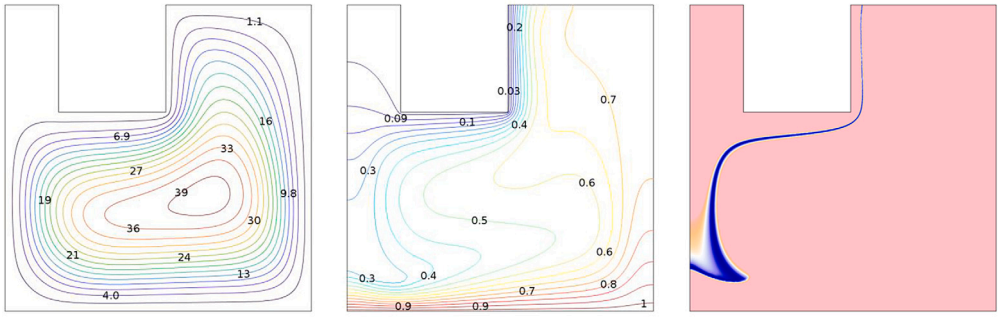

(b) δ = -0.15

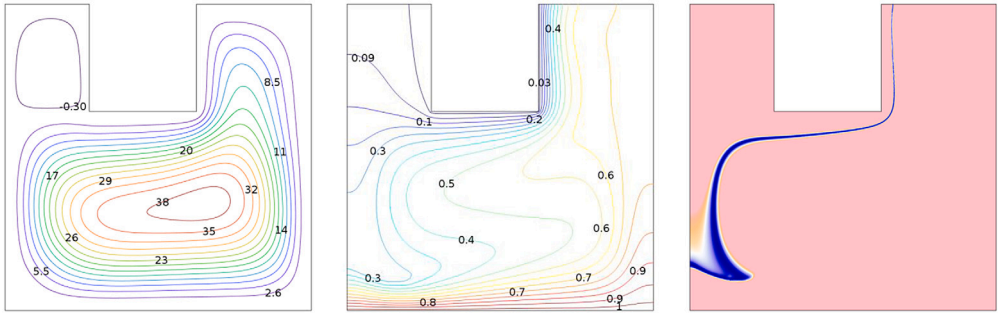

(c) δ = -0.05

Fig. 4. Influence of the asymmetric parameter on streamlines (left), isotherms (middle) and heat capacity ratio distribution (right) at $Ra = 5 \times 10^5$, $\phi = 0.05$, $\theta_f = 0.3$, $Ste = 0.2$ and $AR = 0.35$.

number is low, the heat transfer is dominated by the conduction. Hence, as seen, in Fig. 3(a), the isotherms lay over each other horizontally with minimum deflections. This figure shows almost a conduction heat transfer distribution of temperature from cold to hot. For all cases, the fusion temperature is fixed at the non-dimensional temperature of $\theta_f = 0.3$. In the isotherms of Fig. 3(a), the non-dimensional temperature of $\theta_f = 0.3$ is next to the cold wall and almost lays horizontally. Since the fusion of the nanoparticles takes place at this temperature, a phase change of nanoparticles about this location is expected. The plot of the heat capacity ratio exhibits the phase change region, which is in agreement with the shape and location of the isotherm level of $\theta_f = 0.3$. By the increase of the Rayleigh number, the flow of convection heat transfer gets stronger in the cavity. As seen in the streamlines of Fig. 3(b) for the case of $Ra = 5 \times 10^4$, the hot liquid from the bottom moves upward next to the right wall until it reaches the top wall and then moves along the top cold wall. At the top, the liquid losses its heat to the cold wall and then moves down next to the left wall. Due to the liquid movement (mass transfer), the isotherms have deflected along with the fluid flow, and the isotherm level of $\theta_f = 0.3$ has shifted toward the bottom. The heat capacity ratio also depicts the phase change region in the same location and shape as the mentioned isotherm level. The thickness of the phase change area is under the significant influence of temperature gradients. By the increase of Rayleigh number, the temperature gradients at the core region of the cavity increase, and hence, the general thickness of the phase change area reduces. The temperature gradients can be estimated from a distance between the isotherms. The case of $Ra = 5 \times 10^5$ shows the same trend of behavior as the previous case because both cases represent a convective dominant heat transfer regime. It is interesting that at the bottom of the cavity, the thickness of the phase change area has increased in the convective heat transfer dominant regime. This effect corresponds to the phase change of nanoparticles where there is a smooth flow circulation at that region, and the latent heat of the particles absorbs a notable amount of energy and locally reduces the temperature gradients. The local reduction of temperature gradient leads to the growth of the phase change area.

Fig. 4 shows the evolution of the streamlines, isotherms and heat capacity ratio distribution by adjusting the δ at $Ra = 5 \times 10^5$, $\phi = 0.05$, $\theta_f = 0.3$, $Ste = 0.2$ and $AR = 0.35$. At $\delta = -0.25, -0.15$, single vortex occupies the enclosure. When the center moves to the right approaching the centerline, the single vortex break up into double vortices. Here, the distance between the cold surfaces and the left wall increase that give enough space for the second fluid circulation. As the distance decreases, the shape of the vortex core is elongated horizontally. The location and

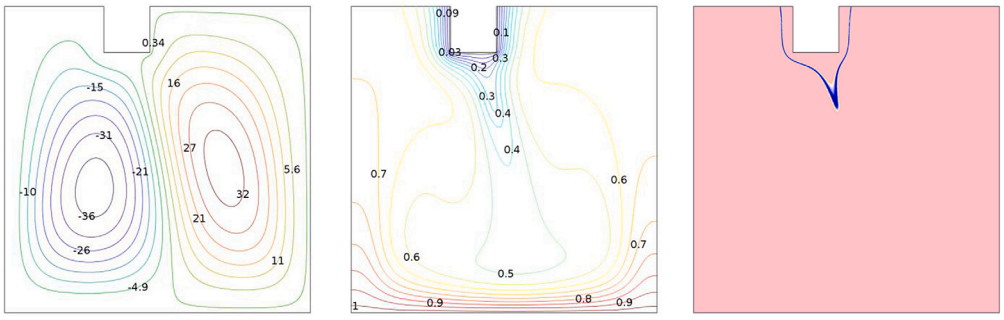

(a) $AR = 0.15$

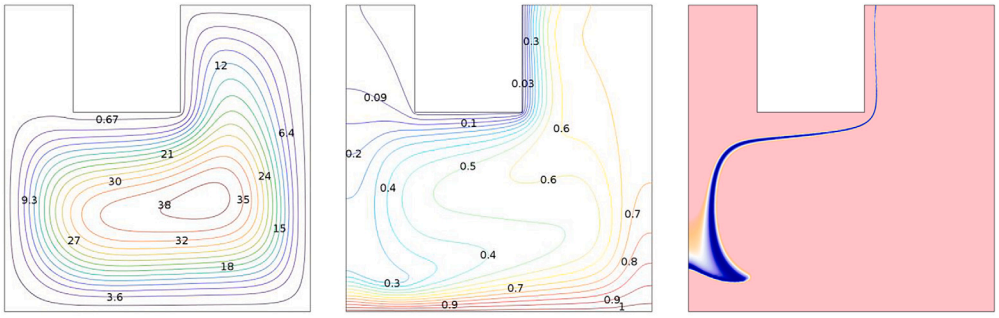

(b) $AR = 0.35$

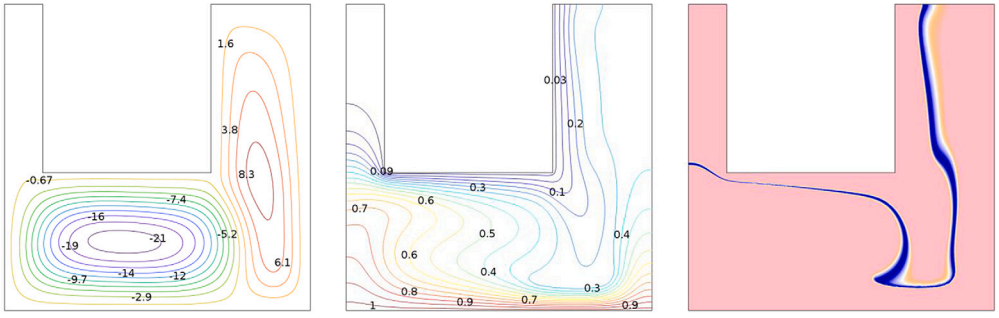

(c) $AR = 0.55$

Fig. 5. Effects of the aspect ratio on streamlines (left), isotherms (middle) and heat capacity ratio distribution (right) at $Ra = 5 \times 10^5$, $\phi = 0.05$, $\theta_f = 0.3$, $Ste = 0.2$ and $\delta = -0.1$. (For interpretation of the references to color in this figure legend, the reader is referred to the web version of this article.)

aspect ratio of the top cold wall controls the direction and dynamic of the natural convection flow. Since the side walls are insulated, the convection heat transfer is controlled by the hot and cold walls at the bottom and top of the cavity. The liquid in the vicinity of the hot wall is warm and light, and hence, it tends to move upward. In contrast, the liquid next to the cold wall is cool and heavy, and hence, it tends to move downward. When the cold wall is exactly at the top center of the cavity (without the asymmetry parameter), both warm and cold liquids compete to move in the opposite direction. In such a case, the Rayleigh–Benard convection cells are expected. The asymmetry parameter deteriorates the balance and helps the convection flow to divide itself into a cold and hot stream. When the gap between the insulated sidewall and the insulated inner wall at the top-right of the cavity reduces, the target liquid gets cold and starts moving downward. The hot liquid also finds its way toward the wide top area at the top-right of the cavity. Hence, as seen, the direction of the convection flow was controlled by the asymmetry parameter. The aspect ratio controllers the size of the top gaps and the distance between the cold and hot walls, and consequently, it controls the dynamic of the natural convection flows. The isotherms will follow the dynamic of the flow circulation. As seen, the change of the isotherms is in agreement with the streamlines. Finally, the phase change area, which is depicted by the heat capacity ratio, takes place around the isotherm level of θ_f, which is equal to the fusion temperature of the nanoparticles.

Fig. 5 shows the evolution of the streamlines, isotherms and heat capacity ratio distribution by increasing the aspect ratio at $Ra = 5 \times 10^5$, $\phi = 0.05$, $\theta_f = 0.3$, $Ste = 0.2$ and $\delta = -0.1$. Two vortices generated by gravitational acceleration occupy enclosure and the shape of the vortex cores is a vertical ellipse at $AR = 0.15$. Thermal plume is appeared near the warm wall. At $AR = 0.35$, the two vortices merge into one and the shape of the core is elongated horizontally. The isotherms become less distorted and the thermal plume is disappeared. In addition, making the aspect ratio greater, the temperature of the fluid adjacent to cold segments decreases because of the narrow space for the fluid circulation. Later at $AR = 0.55$, the two vortices reappear with the strength of fluid circulation is retarded. The isotherms next to the bottom wall become more distorted. As consequence, the boundary layer thickness on the isothermal wall are decreased. This imply increasing the temperature gradient on these surfaces with increasing the aspect ratio. Adjusting the aspect ratio would transform the shape of the heat capacity ratio where the blue line of phase change gets thicker when the enclosure becomes narrower. Flat blue line appears near lower zone of the enclosure and the line thickness looks similar everywhere.

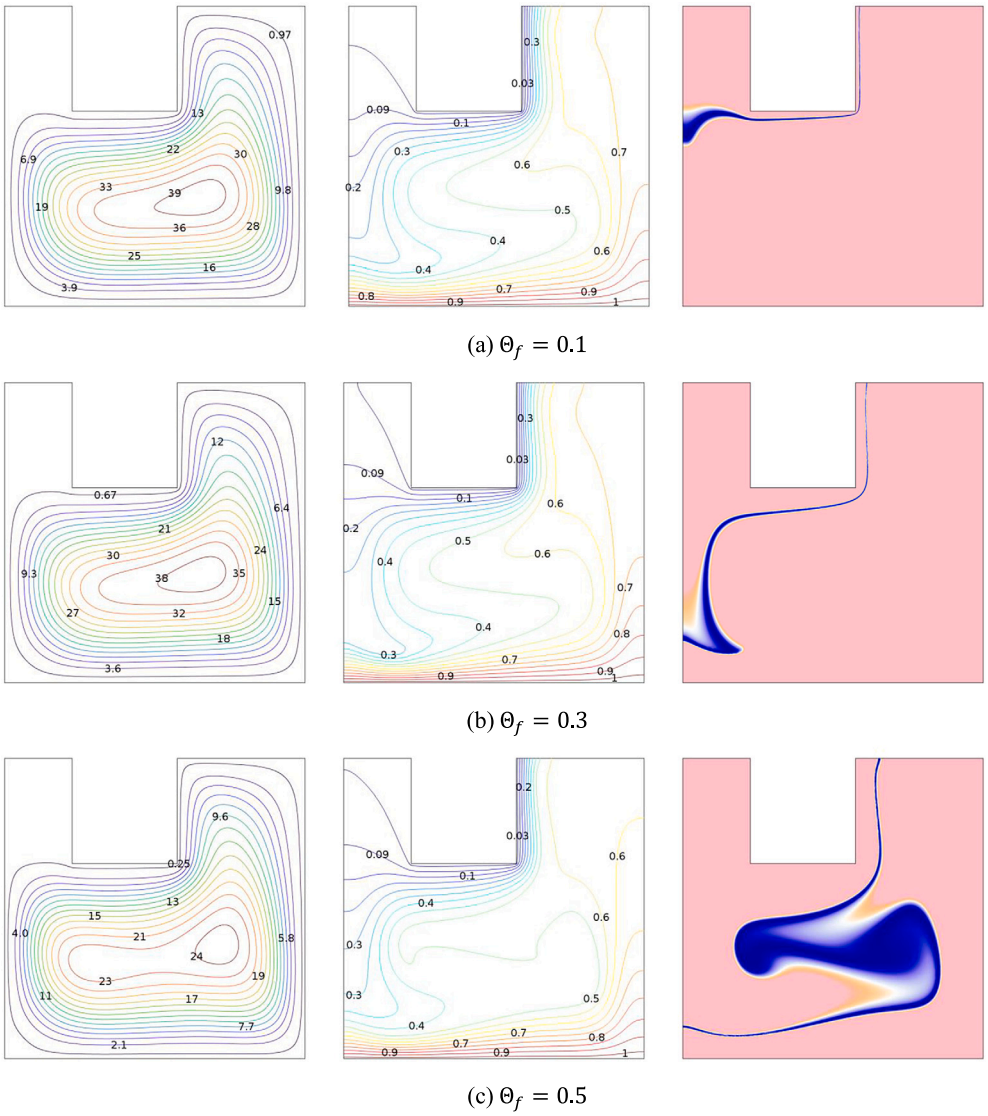

Fig. 6. Influences of the fusion temperature on streamlines (left), isotherms (middle) and heat capacity ratio distribution (right) at $Ra = 5 \times 10^5$, $\phi = 0.05$, $\delta = -0.1$, $Ste = 0.2$ and $AR = 0.35$. (For interpretation of the references to color in this figure legend, the reader is referred to the web version of this article.)

Fig. 6 exhibits the evolution of the streamlines, isotherms and heat capacity ratio distribution by increasing the fusion temperatures at $Ra = 5 \times 10^5$, $\phi = 0.05$, $\delta = -0.1$, $Ste = 0.2$ and $AR = 0.35$. Varying the fusion temperatures inconsiderably affects the streamlines and isotherms. The distribution of temperature at the boundary was not change by varying the θ_f. At $\theta_f = 0.1, 0.3$, the eye of vortex shows an ellipse shape and later at $\theta_f = 0.5$, the ellipse was shortened. The heat capacity ratio exhibits a ribbon-form area near the fixed temperature line of fusion. The blue area displayed in the Cr contours refers to the area of phase change. The ribbon-form of the phase change area is extremely thin adjacent to the right of top U-shaped. This observation justifies the large temperature gradients was revealed at these regions. The blue area gets larger when the fusion temperatures gets higher. When the fusion temperature approximates the hot or cold surfaces temperature, the heat transfer improvement because of the phase change is low. The melting zone moves to right when the fusion temperatures increases. This mechanism indicates that large amount of the NEPCM release their latent heat and solidify.

Fig. 7 illustrates the influence of asymmetric parameter on the local Nusselt number at $Ra = 5 \times 10^5$, $\phi = 0.05$, $\delta = -0.1$, $Ste = 0.2$ and $AR = 0.35$. This figure constitutes the temperature gradient along the heated bottom wall. Obviously, the temperature gradient goes to 1 at right positions of the hot surface. This result conforms the temperature distribution shown in the contour figure. The maximum temperature gradient were obtained near $x = 0.2$. The role of the nano-capsule to the heat transfer variation is quite small near this point for the considered δ because of the surrounding temperature approximates the fusion temperature that indicate the phase change of the core is negligible. The maximum temperature gradient were obtained at $x = 0.15, 0.17, 0.19$, for $\delta = -0.25$, $\delta = -0.15$ and $\delta = -0.05$, respectively. At this location, the surrounding temperature is great distance from the fusion temperature.

Fig. 8 exhibits the influence of the fusion temperature on the Nusselt number contra the center of U-shaped basin location at $Ra = 5 \times 10^5$, $\phi = 0.05$, $Ste = 0.2$ and $AR = 0.35$. The mean Nusselt number is unchanged by adjusting fusion temperature about $\delta = -0.06, 0.06$. The mean Nusselt number was obtained to be maximum at $\theta_f = 0.5$ and $\delta = 0.0$. Considering the symmetric cavity ($\delta = 0.0$), Fig. 8 shows that increasing the non-dimensional fusion temperature from 0.3 to 0.5 promotes the average Nusselt number from 11.1 to 13.2. Hence, choosing phase change materials with proper fusion temperature can improve the heat transfer rate by about 19%. For the same case, reducing the fusion temperature from 0.3 to 0.1 would also promote the heat transfer rate by about 12.5%. This is appropriate by taking into

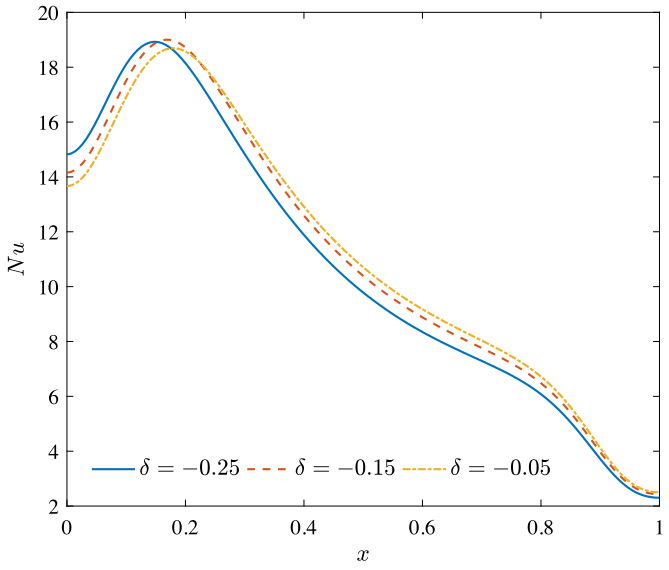

Fig. 7. Effects of the asymmetric parameter on the local Nusselt number at $Ra = 5{\times}10^5$, $\phi = 0.05$, $\delta = -0.1$, $Ste = 0.2$ and $AR = 0.35$.

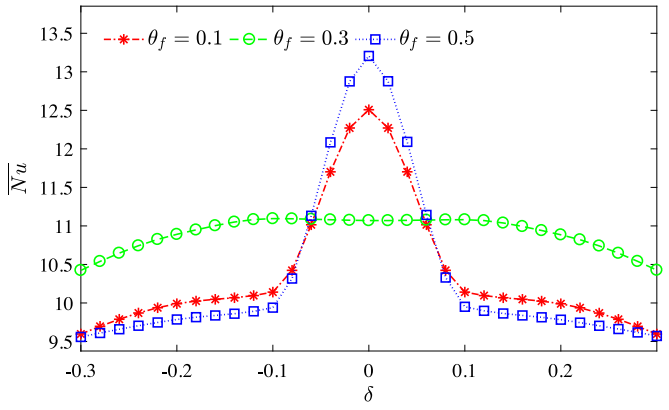

Fig. 8. Influence of the fusion temperature on the mean Nusselt number versus the center of U-shaped basin location at $Ra = 5 \times 10^5$, $\phi = 0.05$, $Ste = 0.2$ and $AR = 0.35$.

account the mechanisms of absorbing, storing and releasing heat for the cases of $\theta_f = 0.5$ at a symmetric U-shaped. Here, the most part of the NEPCMs are in the liquid phase and also the flow rate of suspension passing the phase transition region is insignificant. Here the fusion temperature plays an important role in modifying the heat transfer. Varying the fusion temperature give equal average Nusselt number values at stronger asymmetry case for $\theta_f = 0.1, 0.5$. The geometry parameter have small effect to the Nusselt number for $\theta_f = 0.3$.

Fig. 9 shows the effect of the Stefan number on the mean Nusselt number versus the center of U-shaped basin location at $Ra = 5{\times}10^5$, $\phi = 0.05$, $\theta_f = 0.3$ and $AR = 0.35$. Obviously, the average Nusselt number increase by decreasing the Stefan number. Definitely, if the latent heat of the inner core increase then the Stefan number reduces. Therefore, the smaller the Stefan number, the higher the latent heat. The decrease of Stefan number from 0.4 to 0.2 increased the maximum value of the average Nusselt number from 10.6 to 11.1. Hence, by the reduction of Stefan number to half, the heat transfer was enhanced about 4.7% compared to the case of $Ste = 0.4$. Basin location has a deteriorating effect on heat transfer rate of the system as asymmetry U-shaped leads to larger flow amplification. We observe that symmetry U-shape does not give the highest Nusselt number. The maximum Nusselt number was obtained at $\delta = -0.1, 0.1$.

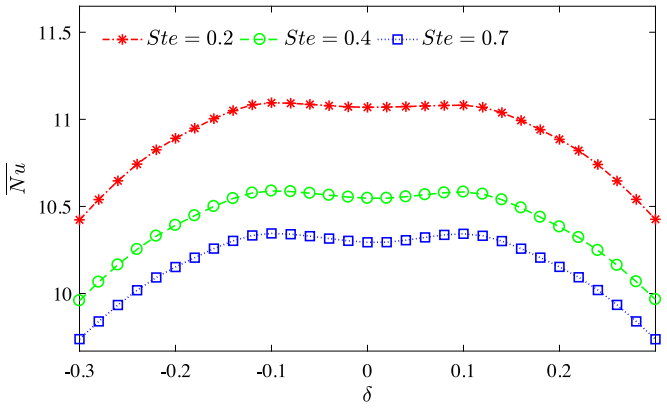

Fig. 9. Effects of the Stefan number on the mean Nusselt number versus the center of U-shaped basin location at $Ra = 5 \times 10^5$, $\delta = -0.1$, $\theta_f = 0.3$ and $AR = 0.35$.

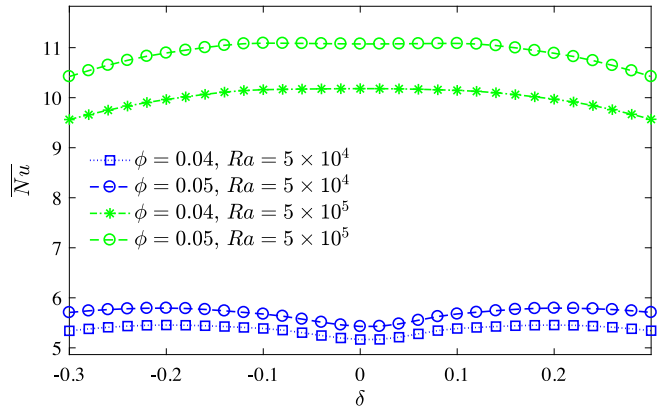

Fig. 10. Impact of the Rayleigh number and NEPCM concentration on the average Nusselt number versus the top U-shaped location at $\phi = 0.04, 0.05$, $Ste = 0.2$, $\theta_f = 0.3$ and $AR = 0.35$.

Fig. 10 exhibits the effect of the Rayleigh number and NEPCM concentration on the average Nusselt number versus the basin location at $Ra = 5{\times}10^4, 5{\times}10^5$, $\phi = 0.04, 0.05$, $Ste = 0.2$, $\theta_f = 0.3$ and $AR = 0.35$. The basin location have small effect to the Nusselt number. Carefully observation indicates that the symmetry U-shaped does not give the highest Nusselt number. The important finding here is an enhancement in the influence of NEPCM concentration on thermal performance by increasing the Rayleigh number. This due to improvement buoyancy and increasing of thermal conductivity ones at high heating intensity. Heat convection dominates at high heating intensity where the NEPCM particles moves with great velocity so that the enhancement in heat transfer enhancement is more pronounced at higher Ra. Here increment 1% nano-capsules volume fraction improves 9% of the heat transfer rate.

Fig. 11 illustrates the effect of aspect ratio on the mean Nusselt number versus the basin location at $Ra = 5 \times 10^5$, $Ste = 0.2$, $\theta_f = 0.3$ and $\phi = 0.05$. The average Nusselt number enhances by enhancing the aspect ratio. This due to when the aspect ratio of the enclosure increases, the U-shaped enclosure becomes narrower and the fluid motion retarded and lead to increasing of heat transfer rate on the bottom wall. Moving of the cold segments to the left or to the right at the same distance gives equal effect on the overall heat transfer. It displays symmetrical curve about $\delta = 0.0$. Basin location is the important aspect for case $AR = 0.15, 0.55$. At this configuration, the stored heat in the capsule significantly modify the lower fluid flow that finally effect the liquid temperature. When the aspect ratio, $AR = 0.35$, the flow is slightly amplified by adjusting the basin location. This

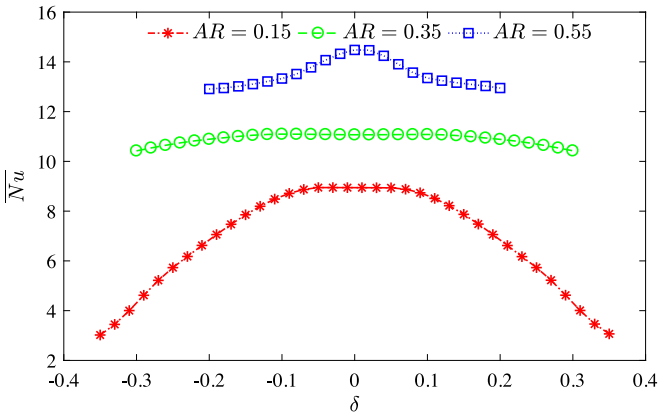

Fig. 11. Influence of the aspect ratio on the mean Nusselt number versus the basin location at $Ra = 5 \times 10^5$, $Ste = 0.2$, $\theta_f = 0.3$ and $\phi = 0.05$.

moderate aspect ratio has dominant flow in the middle region which is less effect to Nusselt number measurement along the bottom wall.

5. Conclusions

The present study scrutinized the impact of NEPCM, asymmetry parameter, magnitude of the temperature difference and the nanoparticles concentration. The equations governing continuity, momentum and energy inside the annulus are stated in the non dimensional form. The latent heat released and absorbed throughout the phase change by the NEPCM is given in the formulation. The partial differential equations of the governing equations are solved numerically by means of the Galerkin finite element method via COMSOL. Local and mean Nusselt numbers is presented graphically. Streamlines, isotherms and heat capacity ratio within the asymmetrical U-shaped are exhibited in contour plot. The fluids are agitated by the melting, asymmetry parameter, heating intensity and the volume fraction parameters. The main conclusions from the investigation are given below:

1. The aspect ratio, fusion temperature, Rayleigh number and location of basin are an essential parameter in the cell number, pattern and its strength.
2. The structure of the isotherm is not affected by the different fusion temperature value but the area of phase change shifts upwards when the fusion temperatures gets higher.
3. Departing of the fusion temperature from the bottom temperatures enhances the successful of the nano-capsule with regard to heat transfer improvement. The maximum heat transfer rate is observed using a fusion temperature about 0.5, low Stefan number, strong Rayleigh number and high NECPM concentration.
4. The global heat transfer performance can be enhanced more than 9% by adding 1% nano-capsules volume fraction. Symmetry U-shaped does not give the maximum heat transfer performance and changing the basin location has small effect the heat transfer enhancement at moderate aspect ratio and fusion temperature.

Examining configuration of the geometry aspect in this work is hoped to be a valuable guide for the experimentalists to study the effectiveness of the NEPCMs capability in storing/releasing an extraordinarily large energy on phase change and it have great potential in the thermal performance and energy harvesting applications.

CRediT authorship contribution statement

H. Saleh: Implemented the ideas. **Z. Siri:** Identified major issues with correctness of the mathematical formulation. **M. Ghalambaz:** Conceived basic idea of the paper.

Declaration of competing interest

The authors declare that they have no known competing financial interests or personal relationships that could have appeared to influence the work reported in this paper.

Acknowledgment

This research was funded by University of Malaya, Malaysia through Impact Oriented Interdisciplinary Research Grant IIRG006C-19IISS. All authors approved the final version of the manuscript.

References

[1] S.U.S. Choi, Enhancing thermal conductivity of fluids with nanoparticles, ASME Fluids Eng. Div. 231 (1995) 99–105.
[2] W. Su, J. Darkwa, G. Kokogiannakis, Review of solid–liquid phase change materials and their encapsulation technologies, Renew. Sustain. Energy Rev. 48 (2015) 373–391.
[3] G. Fang, H. Li, F. Yang, X. Liu, S. Wu, Preparation and characterization of nano-encapsulated n-tetradecane as phase change material for thermal energy storage, Chem. Eng. J. 153 (2009) 217–221.
[4] A. Jamekhorshid, S.M. Sadrameli, M. Farid, A review of microencapsulation methods of phase change materials (PCMs) as a thermal energy storage (TES) medium, Renew. Sustain. Energy Rev. 31 (2014) 531–542.
[5] E.M. Shchukina, M. Graham, Z. Zheng, D.G. Shchukin, Nanoencapsulation of phase change materials for advanced thermal energy storage systems, Chem. Soc. Rev. 47 (2018) 4156–4175.
[6] H. Nazir, M. Batool, F.J.B. sorio, M. Isaza-Ruiz, X. Xu, K. Vignarooban, P. Phelan, Inamuddin, A.M. Kannan, Recent developments in phase change materials for energy storage applications: A review, Int. J. Heat Mass Transf. 129 (2019) 491–523.
[7] Y.S. Morsi, S. Das, Numerical investigation of natural convection inside complex enclosures, Heat Transf. Eng. 24 (2003) 30–41.
[8] K. Khanafer, K. Vafai, M. Lightstone, Buoyancy-driven heat transfer enhancement in a two-dimensional enclosure utilizing nanofluids, Int. J. Heat Mass Transf. 46 (2003) 3639–3653.
[9] R.Y. Jou, S.C. Tzeng, Numerical research of nature convective heat transfer enhancement filled with nanofluids in rectangular enclosures, Int. Commun. Heat Mass Transf. 33 (2006) 727–736.
[10] M. El-Alami, M. Najam, E. Semma, A. Oubarra, F. Penot, Chimney effect in a t form cavity with heated isothermal blocks: The blocks height effect, Energy Convers. Manag. 45 (2004) 3181–3191.
[11] S. Amraqui, A. Mezrhab, C. Abid, Computation of coupled surface radiation and natural convection in an inclined ≪t≫ form cavity, Energy Convers. Manag. 52 (2011) 1166–1174.
[12] A. Kasaeipoor, B. Ghasemi, S.M. Aminossadati, Convection of cu-water nanofluid in a vented T-shaped cavity in the presence of magnetic field, Int. J. Therm. Sci. 94 (2015) 50–60.
[13] T. Armaghani, A. Kasaeipoor, M. Izadi, I. Pop, MHD natural convection and entropy analysis of a nanofluid inside T-shaped baffled enclosure, Int. J. Numer. Methods Heat Fluid Flow 28 (2018) 2916–2941.
[14] A.J. Chamkha, M. Ismael, A. Kasaeipoor, T. Armaghani, Entropy generation and natural convection of cuo-water nanofluid in C-shaped cavity under magnetic field, Entropy 18 (2016) 50.
[15] B. Mliki, M.A. Abbassi, A. Omri, Z. Belkacem, Lattice Boltzmann analysis of mhd natural convection of cuo-water nanofluid in inclined C-shaped enclosures under the effect of nanoparticles brownian motion, Powder Technol. 308 (2017) 70–83.
[16] R. Mohebbi, M. Izadi, A.J. Chamkha, Heat source location and natural convection in a C-shaped enclosure saturated by a nanofluid, Phys. Fluids 29 (2017) 122009.
[17] S. Aghakhani, A.H. Pordanjani, A. Karimipour, A. Abdollahi, M. Afrand, Numerical investigation of heat transfer in a power-law non-Newtonian fluid in a C-shaped cavity with magnetic field effect using finite difference lattice Boltzmann method, Comput. Fluids 176 (2018) 51–67.
[18] A. Abedini, T. Armaghani, A.J. Chamkha, MHD free convection heat transfer of a water-fe3o4 nanofluid in a baffled C-shaped enclosure, J. Therm. Anal. Calorim. 135 (2019) 685–695.
[19] A. Rahimi, M. Sepehr, M.J. Lariche, M. Mesbah, A. Kasaeipoor, E.H. Malekshah, Analysis of natural convection in nanofluid-filled H-shaped cavity by entropy generation and heatline visualization using lattice boltzmann method, Physica E 97 (2018) 347–362.
[20] A. Purusothaman, E.H. Malekshah, Lattice Boltzmann modeling of MHD free convection of nanofluid in a V-shaped microelectronic module, Therm. Sci. Eng. Prog. 10 (2019) 186–197.
[21] M. Kalteh, H. Hasani, Lattice Boltzmann simulation of nanofluid free convection heat transfer in an L-shaped enclosure, Superlattices Microstruct. 66 (2014) 112–128.

[22] H.M. Elshehabey, F.M. Hady, S.E. Ahmed, R.A. Mohamed, Numerical investigation for natural convection of a nanofluid in an inclined L-shaped cavity in the presence of an inclined magnetic field, Int. Commun. Heat Mass Transf. 57 (2014) 228–238.
[23] R. Mohebbi, M.M. Rashidi, Numerical simulation of natural convection heat transfer of a nanofluid in an L-shaped enclosure with a heating obstacle, J. Taiwan Inst. Chem. Eng. 72 (2017) 70–84.
[24] A. Rahimi, A. Kasaeipoor, E.H. Malekshah, A. Amiri, Natural convection analysis employing entropy generation and heatline visualization in a hollow L-shaped cavity filled with nanofluid using lattice Boltzmann method-experimental thermo-physical properties, Physica E 97 (2018) 82–97.
[25] Amitkumar S. Gawas, Dhiraj V. Patil, Rayleigh-bénard Type natural convection heat transfer in two-dimensional geometries, Appl. Therm. Eng. 153 (2019) 543–555.
[26] C.C. Cho, H.T. Yau, C.H. Chiu, K.C. Chiu, Numerical investigation into natural convection and entropy generation in a nanofluid-filled U-shaped cavity, Entropy 17 (2015) 5980–5994.
[27] Y. Ma, R. Mohebbi, M.M. Rashidi, Z. Yang, Simulation of nanofluid natural convection in a U-shaped cavity equipped by a heating obstacle: Effect of cavity's aspect ratio, J. Taiwan Inst. Chem. Eng. 93 (2018) 263–276.
[28] L. Snoussi, N. Ouerfelli, X. Chesneau, A.J. Chamkha, A. Belgacem, F.M. Guizani, Natural convection heat transfer in a nanofluid filled U-shaped enclosures: numerical investigations, Heat Transf. Eng. 39 (2018) 1450–1460.
[29] Y. Ma, R. Mohebbi, M.M. Rashidi, Z. Yang, Mixed convection characteristics in a baffled U-shaped lid-driven cavity in the presence of magnetic field, J. Taiwan Inst. Chem. Eng. (2019) 1–18.
[30] S.S. Sebti, M. Mastiani, H. Mirzaei, A. Dadvand, S. Kashani, S.A. Hosseini, Numerical study of the melting of nano-enhanced phase change material in a square cavity, J. Zhejiang Univ. Sci. A 14 (2013) 307–316.
[31] C.J. Ho, J.Y. Gao, An experimental study on melting heat transfer of paraffin dispersed with al2o3 nanoparticles in a vertical enclosure, Int. J. Heat Mass Transf. 62 (2013) 2–8.
[32] S.H. Tasnim, R. Hossain, S. Mahmud, A. Dutta, Convection effect on the melting process of nano-PCM inside porous enclosure, Int. J. Heat Mass Transf. 85 (2015) 206–220.
[33] M. Gurturk, A. Koca, H.F. Oztop, Y. Varol, M. Sekerci, Energy and exergy analysis of a heat storage tank with a novel eutectic phase change material layer of a solar heater system, Int. J. Green Energy 14 (2017) 1073–1080.
[34] N.S. Dhaidan, Nanostructures assisted melting of phase change materials in various cavities, Appl. Therm. Eng. 111 (2017) 193–212.
[35] M. Ghalambaz, A. Doostani, A.J. Chamkha, M.A. Ismael, Melting of nanoparticles-enhanced phase-change materials in an enclosure: effect of hybrid nanoparticles, Int. J. Mech. Sci. 134 (2017) 85–97.
[36] M. Ghalambaz, A. Doostani, E. Izadpanahi, A.J. Chamkha, Phase-change heat transfer in a cavity heated from below: the effect of utilizing single or hybrid nanoparticles as additives, J. Taiwan Inst. Chem. Eng. 72 (2017) 104–115.
[37] S. Motahar, A.A. Alemrajabi, R. Khodabandeh, Experimental investigation on heat transfer characteristics during melting of a phase change material with dispersed tio2 nanoparticles in a rectangular enclosure, Int. J. Heat Mass Transf. 109 (2017) 134–146.
[38] M. Al-Jethelah, S.H. Tasnim, S. Mahmud, A. Dutta, Melting of nano-PCM in an enclosed space: Scale analysis and heatline tracking, Int. J. Heat Mass Transf. 119 (2018) 841–859.
[39] F. Selimefendigil, H.F. Oztop, A.J. Chamkha, Natural convection in a cuo-water nanofluid filled cavity under the effect of an inclined magnetic field and phase change material (PCM) attached to its vertical wall, J. Therm. Anal. Calorim. 135 (2019) 1577–1594.
[40] N.S. Bondareva, B. Buonomo, O. Manca, M.A. Sheremet, Heat transfer performance of the finned nano-enhanced phase change material system under the inclination influence, Int. J. Heat Mass Transf. 135 (2019) 1063–1072.
[41] F. Iachachene, Z. Haddad, H.F. Oztop, E. Abu-Nada, Melting of phase change materials in a trapezoidal cavity: Orientation and nanoparticles effects, J. Mol. Liq. 292 (2019) 110592.
[42] F. Selimefendigil, H.F. Oztop, Mixed convection in a PCM filled cavity under the influence of a rotating cylinder, Sol. Energy 200 (2020) 61–75.
[43] M. Ghalambaz, A.J. Chamkha, D. Wen, Natural convective flow and heat transfer of nano-encapsulated phase change materials (NEPCMs) in a cavity, Int. J. Heat Mass Transf. 138 (2019) 738–749.
[44] A. Hajjar, S.A.M. Mehryan, M. Ghalambaz, Time periodic natural convection heat transfer in a nano-encapsulated phase-change suspension, Int. J. Mech. Sci. 166 (2020) 105243.
[45] S.M.H. Zadeh, S.A.M. Mehryan, M. Sheremet, M. Ghodrat, M. Ghalambaz, Thermo-hydrodynamic and entropy generation analysis of a dilute aqueous suspension enhanced with nano-encapsulated phase change material, Int. J. Mech. Sci. (2020) 105609.
[46] S.A.M. Mehryan, M. Ghalambaz, L.S. Gargari, A. Hajjar, M. Sheremet, Natural convection flow of a suspension containing nano-encapsulated phase change particles in an eccentric annulus, J. Energy Storage 28 (2020) 101236.
[47] M. Ghalambaz, J. Zhang, Conjugate solid–liquid phase change heat transfer in heatsink filled with phase change material-metal foam, Int. J. Heat Mass Transf. 146 (2020) 118832.
[48] S. Barlak, O.M. Sara, A. Karaipekli, S. Yapıcı, Thermal conductivity and viscosity of nanofluids having nanoencapsulated phase change material, Nanosc. Microsc. Therm. 20 (2016) 85–96.
[49] L. Chai, R. Shaukat, L. Wang, H.S. Wang, A review on heat transfer and hydrodynamic characteristics of nano/microencapsulated phase change slurry (n/MPCS) in mini/microchannel heat sinks, Appl. Therm. Eng. 135 (2018) 334–349.
[50] Q. Li, K. Ito, Z. Wu, C.S. Lowry, S.P. Loheide, COMSOL multiphysics: A novel approach to ground water modeling, Groundwater 47 (2009) 480–487.
[51] O.C. Zienkiewicz, R.L. Taylor, P. Nithiarasu, The finite element method for fluid dynamics, in: The Finite Element Method for Fluid Dynamics, seventh ed., Butterworth-Heinemann, Oxford, 2014.
[52] B. Ghasemi, Magnetohydrodynamic natural convection of nanofluids in U-shaped enclosures, Numer. Heat Transf. Part A 63 (2013) 473–487.
[53] A. Mansour, A.Y. Bakier, M. Bakier, Natural convection of the localized heat sources of T-shaped nanofluid-filled enclosures, Am. J. Eng. Res. 2 (2013) 49–61.